

**OFFICIAL USE ONLY**

Enclosure 1: #58

SANDIA REPORT

SAND88 - 1497  
Printed November 1988

Unique Document # SAB20008780000

# Ground Shock from Earth Penetrator Weapons

Paul Yarrington

CONFIRMED TO BE UNCLASSIFIED  
AUTHORITY DOE/RN-52  
BY R.H. SMILEY  
RHS, ADD, 2-22-96

Prepared by  
Sandia National Laboratories  
Albuquerque, New Mexico 87185 and Livermore, California 94550  
for the United States Department of Energy  
under Contract DE-AC04-76DP00789

CONFIRMED TO BE UNCLASSIFIED  
DOE/OCCIE  
BY: NC Nancy Connelly, ADD (DR. 80-10)  
Date: 4/5/05  
HRV/mrb 5/11/07

**OFFICIAL USE ONLY**

Issued by Sandia National Laboratories, operated for the United States Department of Energy by Sandia Corporation.

**NOTICE:** This report was prepared as an account of work sponsored by an agency of the United States Government. Neither the United States Government nor any agency thereof, nor any of their employees, nor any of their contractors, subcontractors, or their employees, makes any warranty, express or implied, or assumes any legal liability or responsibility for the accuracy, completeness, or usefulness of any information, apparatus, product or process disclosed, or represents that its use would not infringe privately owned rights. Reference herein to any specific commercial product, process, or service by trade name, trademark, manufacturer, or otherwise, does not necessarily constitute or imply its endorsement, recommendation, or favoring by the United States Government, any agency thereof or any of their contractors or subcontractors. The views and opinions expressed herein do not necessarily state or reflect those of the United States Government, any agency thereof or any of their contractors.

~~OFFICIAL USE ONLY~~

SAND88-1497  
OFFICIAL USE ONLY  
Printed November 1988

## Ground Shock from Earth Penetrator Weapons

Paul Yarrington  
Computational Physics & Mechanics Division II  
Sandia National Laboratories  
Albuquerque, New Mexico

### ABSTRACT

This report presents results of calculations to predict ground shock effects from earth penetrating weapons. The study models 500 kiloton explosions at two depths below the ground surface in homogeneous, saturated, soft rock geology. Comparisons of weapon lethal range are made using various free-field damage criteria for near-surface and deeply-buried targets. Comparisons are also made with calculational results for ground shock from above-surface and shallowly-buried selected bursts.

~~OFFICIAL USE ONLY~~

## Contents

<b>1. Introduction</b>	<b>1</b>
<b>2. Calculational Approach</b>	<b>2</b>
<b>3. Calculational Results and Description of Phenomenology</b>	<b>7</b>
<b>4. Comparison of Ground Shock Effects</b>	<b>17</b>
<b>5. Discussion</b>	<b>29</b>
<b>6. Acknowledgements</b>	<b>30</b>
<b>7. References</b>	<b>31</b>
<b>APPENDIX</b>	<b>32</b>

## List of Figures

1	Hugoniot curves for wet tuff model. . . . .	3
2	Hugoniot and release curves for wet tuff model. ( $P_r$ is the shock pressure from which release occurs.) . . . . .	4
3	One megabar pressure contour for 6m DOB EPW at 50 $\mu$ sec. . . . .	9
4	Sequence of early time pressure contours for 6m DOB EPW. . . . .	10
5	Velocity and temperature profiles on axis for 6m DOB EPW. . . . .	11
6	Energy partitioning between ground and air for 6m DOB EPW. . . . .	12
7	Pressure contours for 6m DOB EPW and 12m DOB EPW. . . . .	13
8	Energy history in air for EPW bursts. . . . .	14
9	Pressure decay at center of burst for EPW and fully-contained explosions. . . . .	15
10	Late-time pressure contours for EPW bursts. . . . .	16
11	Comparison of 0.5 kb peak axial stress contours for EPW bursts. . . . .	18
12	Comparison of 1.0 kb peak axial stress contours for EPW bursts. . . . .	19
13	Comparison of 0.5 kb peak axial stress contours for above-surface and EPW bursts. . . . .	20
14	Comparison of 1.0 kb peak axial stress contours for above-surface and EPW bursts. . . . .	21
15	Peak stress on axis versus depth for EPW bursts and fully-contained explosion. . . . .	24
16	Peak stress attenuation on axis for EPW and near-surface bursts. . . . .	25
17	Yield factor as function of burst position. . . . .	26
18	Comparison of 6 m/s peak horizontal velocity contours for EPW bursts. . . . .	27
19	Comparison of 0.5 kb peak horizontal stress contours for EPW bursts. . . . .	28



## 2. Computational Approach

The calculations reported here were performed with the two-dimensional, Eulerian wavecode, CSQII (version 6/82) [3], assuming cylindrical symmetry about the penetrator axis. The penetrator was modeled as a solid cylinder of iron, 30 cm in diameter and 180 cm long. The center of the penetrator was assumed to be at the nominal depth of burst for each problem. Energy release for the the EPW burst was simulated by uniformly depositing 500 kt ( $2.1 \times 10^{22}$  ergs) of energy in the iron cylinder representing the penetrator, with the energy being deposited at a constant rate over a time interval of 20 nanoseconds.

The effects of the penetration event on the target material above the weapon were assumed to be of negligible importance to the energy coupling and ground shock associated with the EPW bursts. Thus, the target medium surrounding the weapon in all directions was modeled as uniform and undisturbed. Air above the ground surface was explicitly modeled in the calculations.

The ANEOS [4] equation-of-state (EOS) package associated with CSQ was used to model the materials in the calculations. A library EOS (ANEOS Library Material No. -5) was used for the iron penetrator, although, given the extremely high temperatures reached by the penetrator materials, the ground shock effects are essentially independent of the material chosen to model the projectile. A tabular EOS (Table No. 1885) was used for the air. The ANEOS input for the tuff is given in Appendix 1, while principal material properties are listed in Table 1. Material properties for the tuff were chosen to be the same as those used in an earlier Sandia calculational study [5] of ground shock effects. Hugoniot and selected release curves generated with the tuff model are shown in Figures 1 and 2.



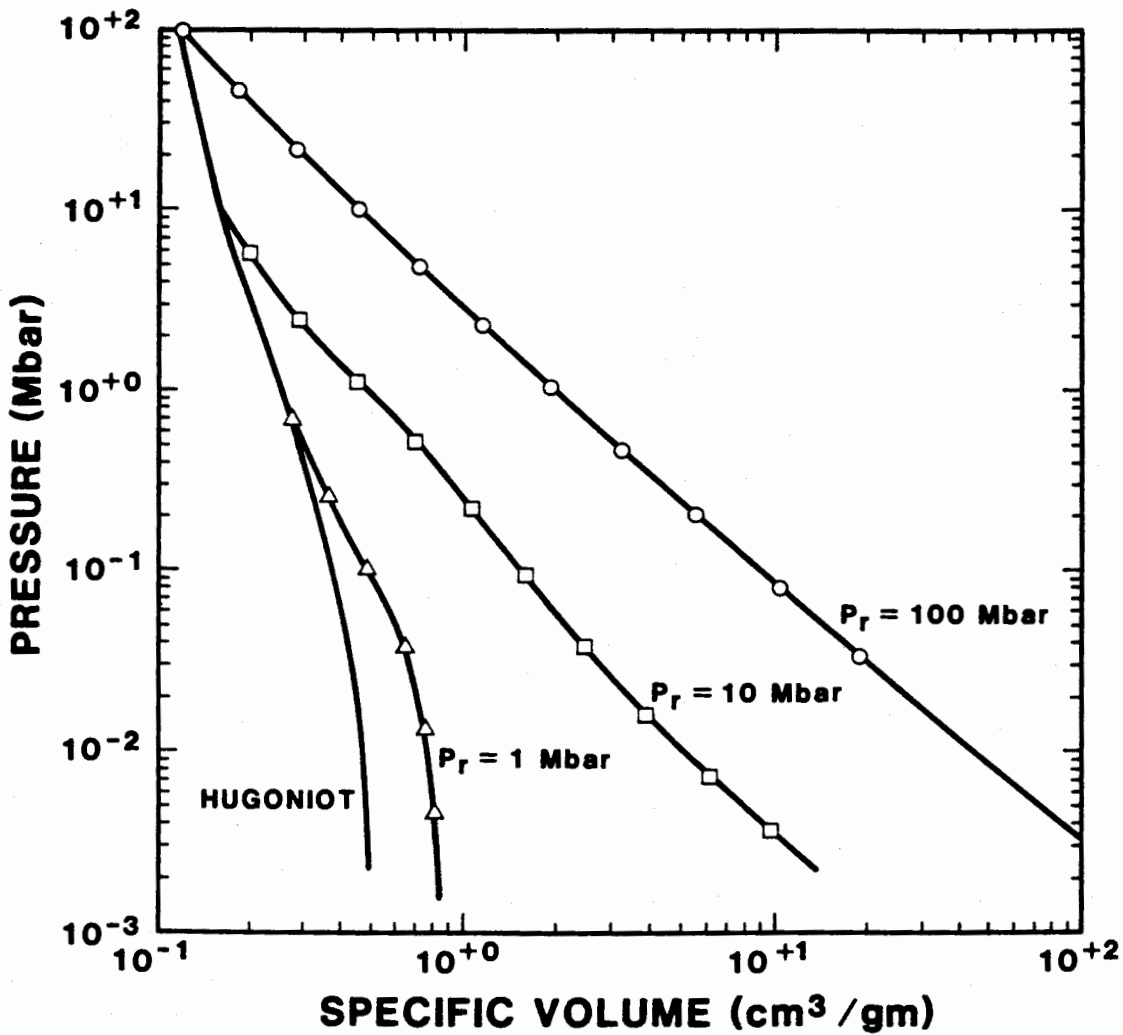


Figure 2: Hugoniot and release curves for wet tuff model. (P<sub>r</sub> is the shock pressure from which release occurs.)

Property	Symbol	Value
Initial Density	$\rho_0$	2.0 gm/cc
Sound speed	$C_0$	$2.8 \times 10^5$ cm/sec
Poisson's ratio	$\mu$	0.31
Mises limit	$Y_m$	0.3 Kbar
Yield constant	$k$	$3.1 \text{ Kbar}^{-1}$

The yield strength for the tuff was assumed to be pressure-dependent, with the yield surface having the form

$$Y(P) = Y_m(1 - e^{-kP}) .$$

The strength constants  $Y_m$  and  $k$  used for the tuff are given in Table 1. The pressure,  $P$ , in this relation is calculated from

$$P = \rho c^2 \eta ,$$

where  $\rho$  and  $c$  are, respectively, the current density and sound speed of the material, and

$$\eta = 1 - \rho_0/\rho .$$

The deviatoric stress state in the material is limited by the yield surface,  $Y(P)$ , calculated from the relation above, as described in Sect. II-4 of the CSQ documentation [3]. Since this pressure-dependent strength model is not a standard option in CSQ, the updates that were used to implement it in the code are included in the Appendix.

The initial zoning for the problem employed uniform, 5 cm square zones, to a radius of 5 meters (100 zones) from the center of the explosion. Shortly before the shock wave from the burst reached the edge of the initial mesh, the problem was rezoned by doubling the zone size and the overall dimensions of the calculational grid. This zoning/rezoning approach, in which square zones are used in the ground shock region, with 100 zones in each direction (horizontally outward and vertically downward) from

the burst, and in which the zone size is doubled when the disturbance reaches the edge of the mesh, was used throughout the calculations. The procedure provides a minimum of 50 zones between the original center of the burst and the leading edge of the ground shock at all times during the calculations. Above the ground surface, zones were allowed to increase in vertical dimension by a constant ratio (always less than 5 percent) as the vertical distance increased. The calculations were rezoned eight times, as indicated in Table 2, to reach the final problem time of 0.3 seconds.

**TABLE 2**

**Zoning for EPW Calculations**

Time	Shock Radius	Zone Size*
0 - 30 usec	0 - 5 m	5 cm
30 - 200 usec	5 - 10 m	10 cm
200 - 800 usec	10 - 20 m	20 cm
0.8 - 4 ms	20 - 40 m	40 cm
4 - 12 ms	40 - 80 m	80 cm
12 - 35 ms	80 - 160 m	160 cm
35 - 80 ms	160 - 320 m	320 cm
80 - 175 ms	320 - 640 m	640 cm

\*Zone size refers to side length in square-zoned region of mesh extending 100 zones horizontally outward and 100 zones vertically downward from the center of burst.

### 3. Calculational Results and Description of Phenomenology

Within a few microseconds after the burst, the expanding cavity of vaporized tuff and weapon debris becomes essentially spherical. This can be seen in Figure 3, which shows the 1 Mbar pressure contour for the 6 m DOB problem at 50 microseconds, shortly before the burst breaks through the surface of the ground. Note that the center of burst was at the origin of the coordinate system in both of the EPW calculations. When breakout occurs, energy is rapidly lost from the cavity, as hot, high pressure gases vent to the atmosphere. Figure 4 shows a sequence of early-time pressure contours, where the strong hydrodynamic motions that occur following breakout are evident. Velocity and temperature profiles on axis during this cavity breakout phase of the problem are shown in Figure 5. Histories of total energy in the tuff and in the air are cross-plotted to a problem time of 10 ms in Figure 6, where the rapid, early-time transfer of energy from tuff to air can be clearly seen.

For the deeper burst, these processes occur later in time, and less energy is transferred to the air than for the shallower burst. Figure 7 compares pressure contours for the two EPW bursts at problem times of 2 ms, 6 ms and 10 ms. Figure 8 shows the time history of total energy in the air during the first 30 ms for the two problems. As time progresses, the pressure in the cavity for both bursts drops well below that for a fully-contained explosion [6], as shown in Figure 9.

Figure 10 compares late-time pressure contours for both problems and shows a somewhat stronger ground shock for the deeper burst, as would be expected. This is evident from the wider contours that are seen for the deeper burst at any given stress level. Compare, for example, the 0.5 kb contours (level E) for the two cases.

With the contour levels chosen in Figure 10, the front of a pressure wave can be seen propagating in the air along the ground surface, suggesting that some "airblast" effects may be associated with the EPW bursts. The strength of this blast wave is

OFFICIAL USE ONLY

greatly reduced, however, from that produced by a surface burst and will decay to negligible levels at ranges where the ground shock is still well above its lethal level. Thus, ground shock is definitely the dominant weapon effect against hardened structures for the EPW bursts simulated here, with "airblast" making virtually no contribution to the overall lethal radius of the weapon.

OFFICIAL USE ONLY



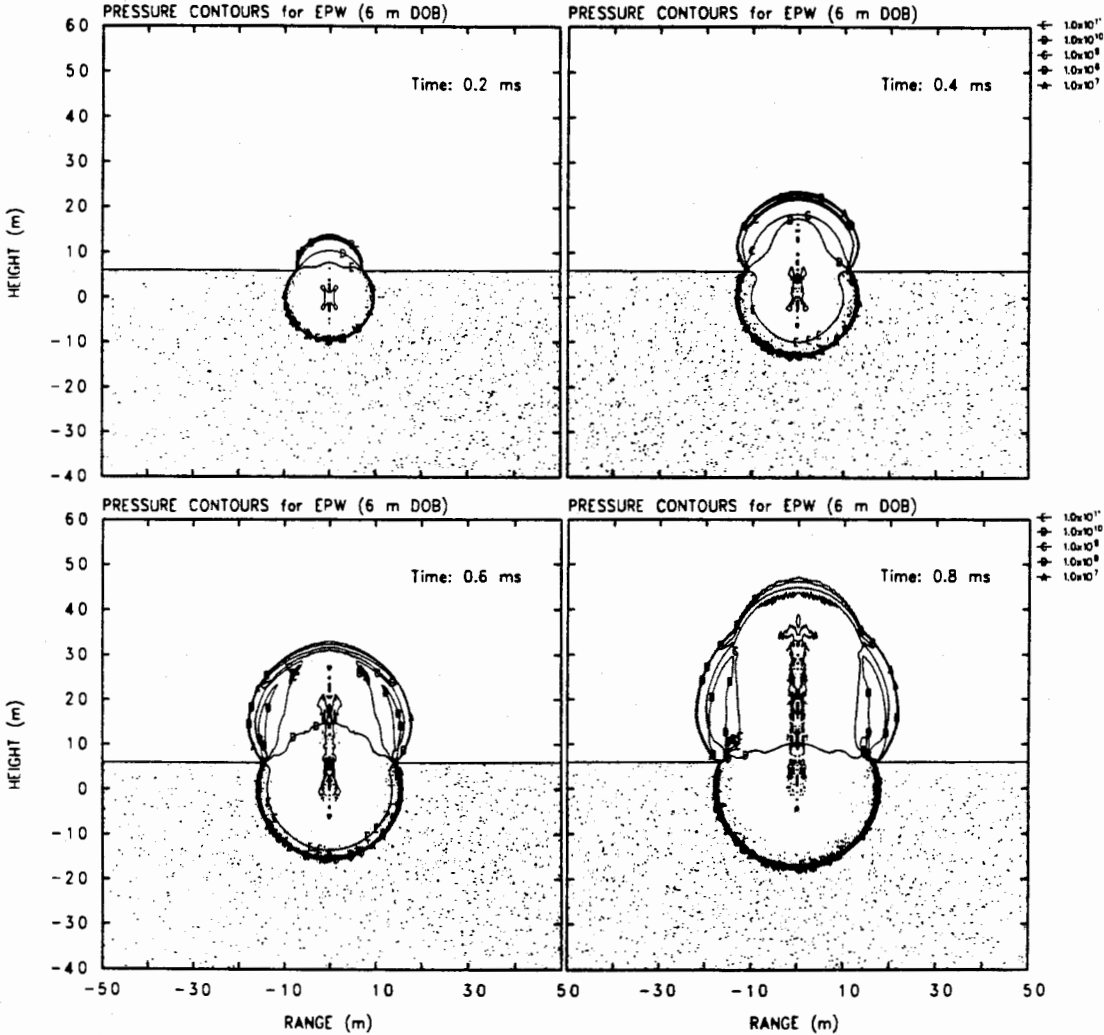


Figure 4: Sequence of early time pressure contours for 6m DOB EPW, showing rapid venting from cavity to air. Contour levels (in Pa) indicated at the right.

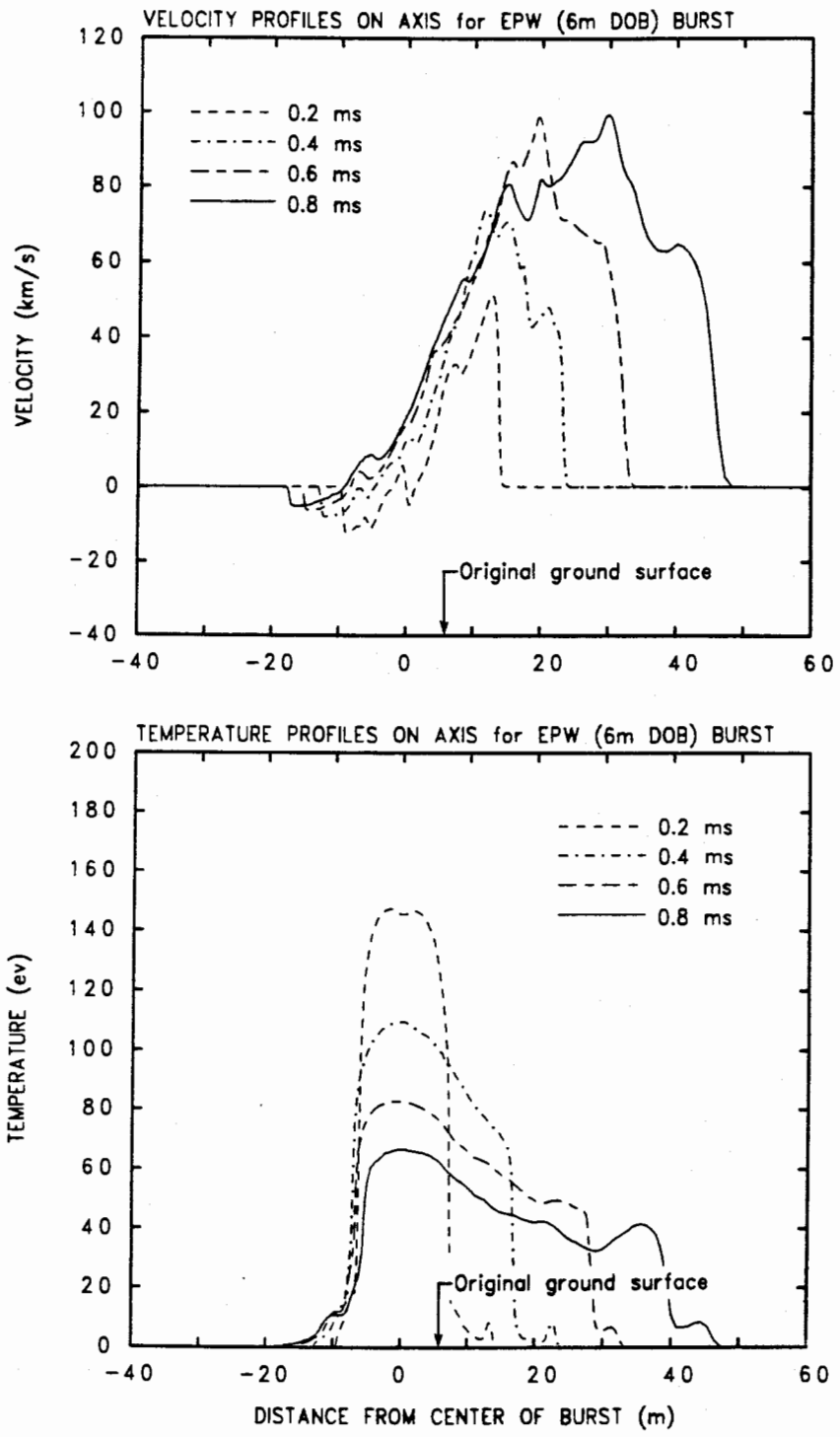


Figure 5: Velocity and temperature profiles on axis for 6m DOB EPW during cavity venting phase of problem.

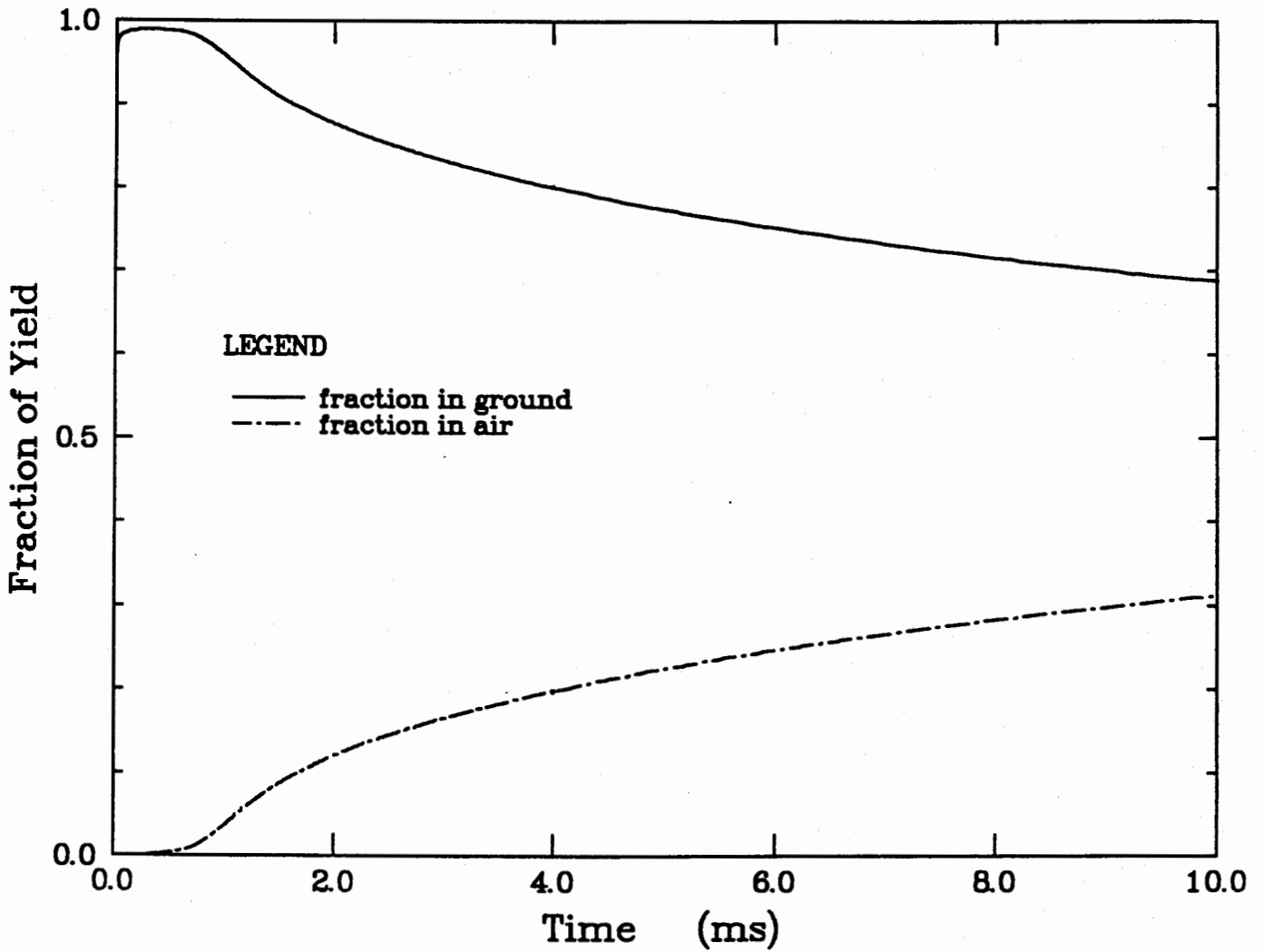


Figure 6: Energy partitioning between ground and air for 6m DOB EPW.



OFFICIAL USE ONLY

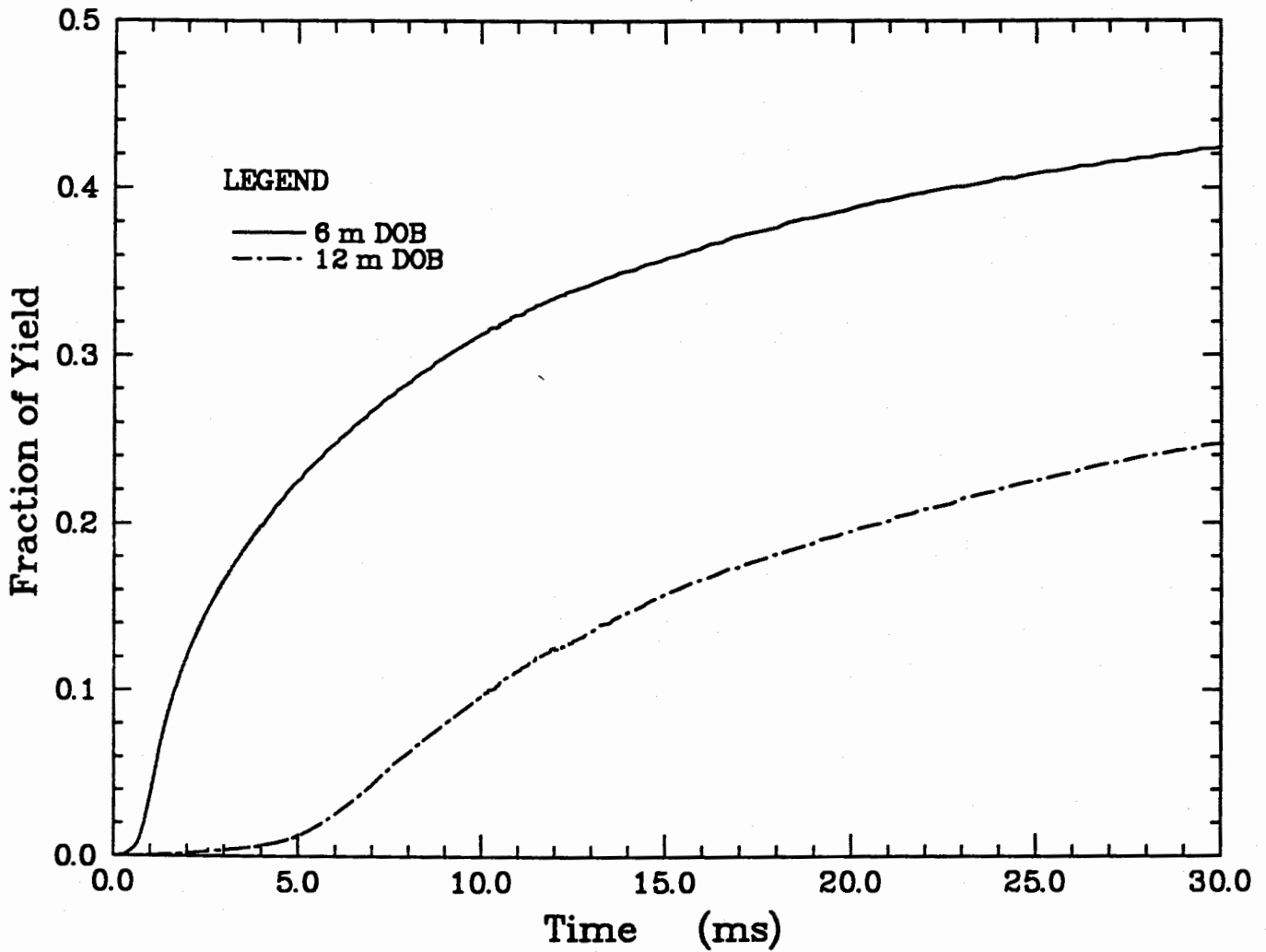


Figure 8: Energy history in air for EPW bursts.

OFFICIAL USE ONLY

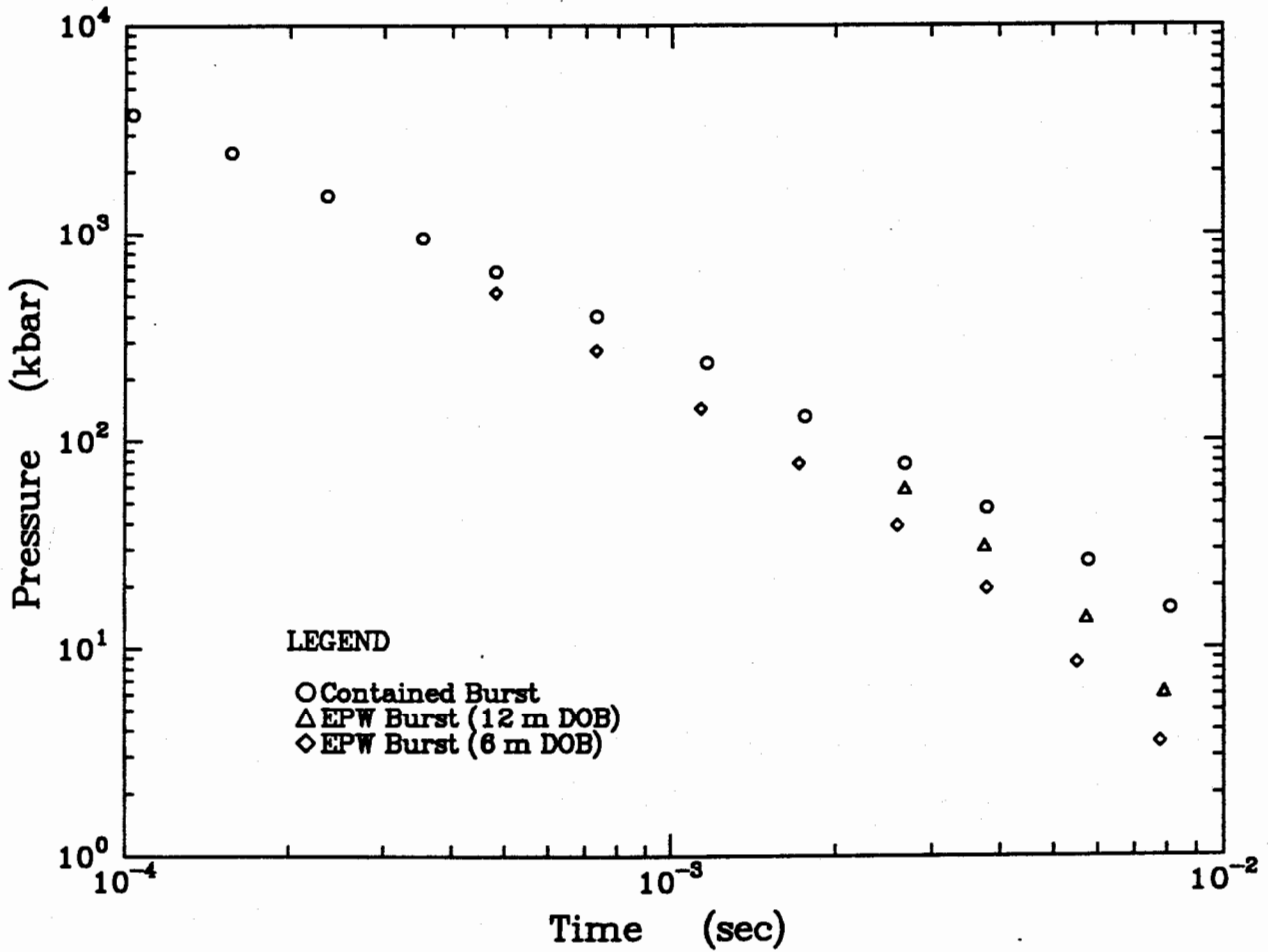


Figure 9: Pressure decay at center of burst for EPW and fully-contained explosions.







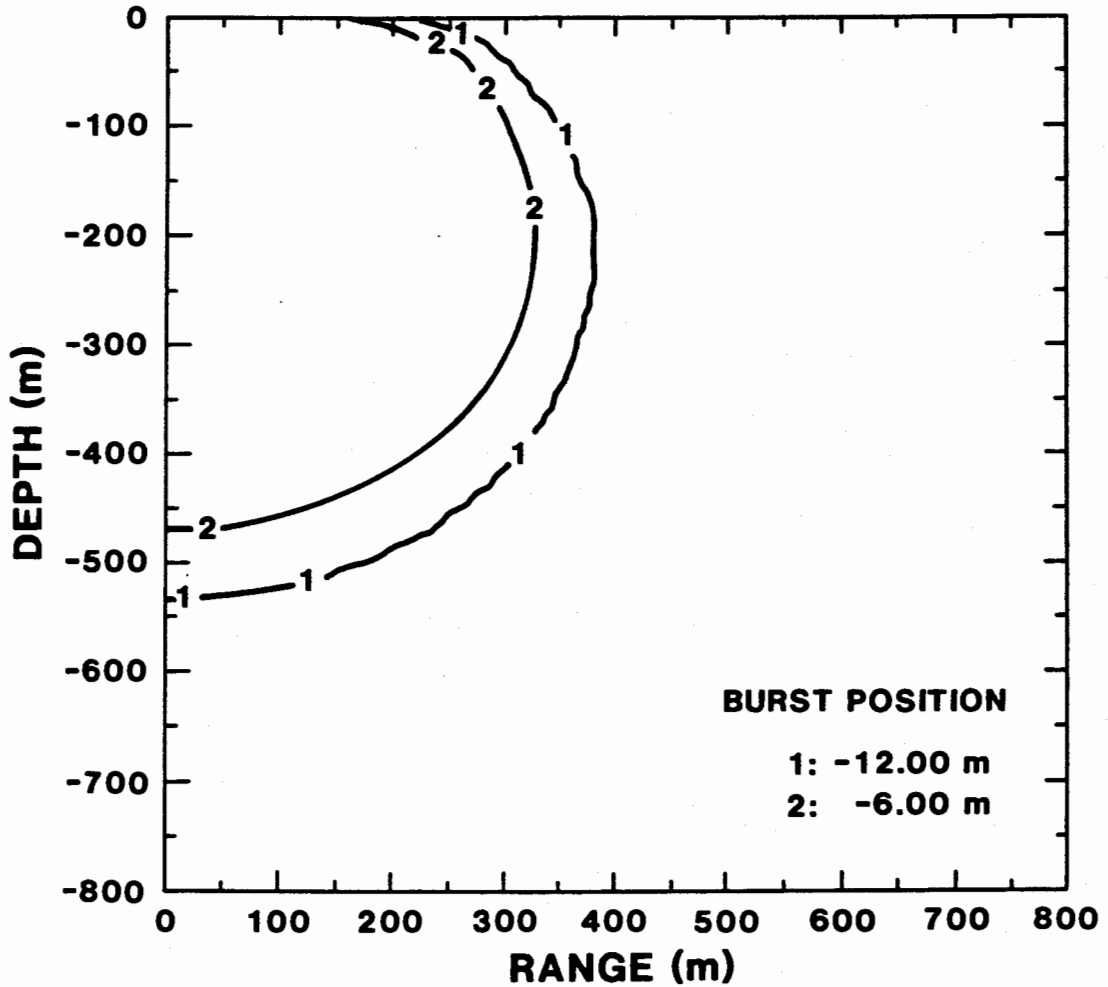


Figure 12: Comparison of 1.0 kb peak axial stress contours for EPW bursts.

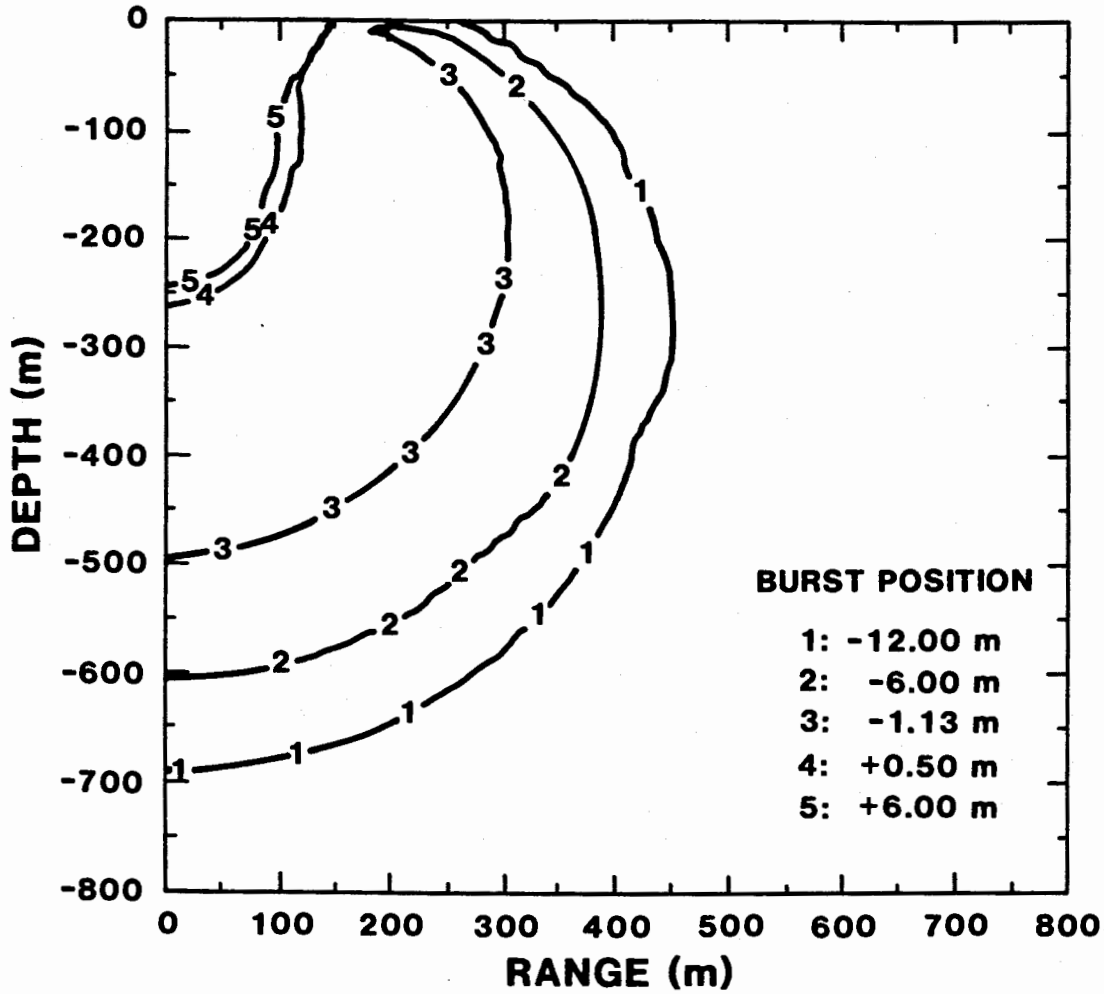


Figure 13: Comparison of 0.5 kb peak axial stress contours for above-surface and EPW bursts.







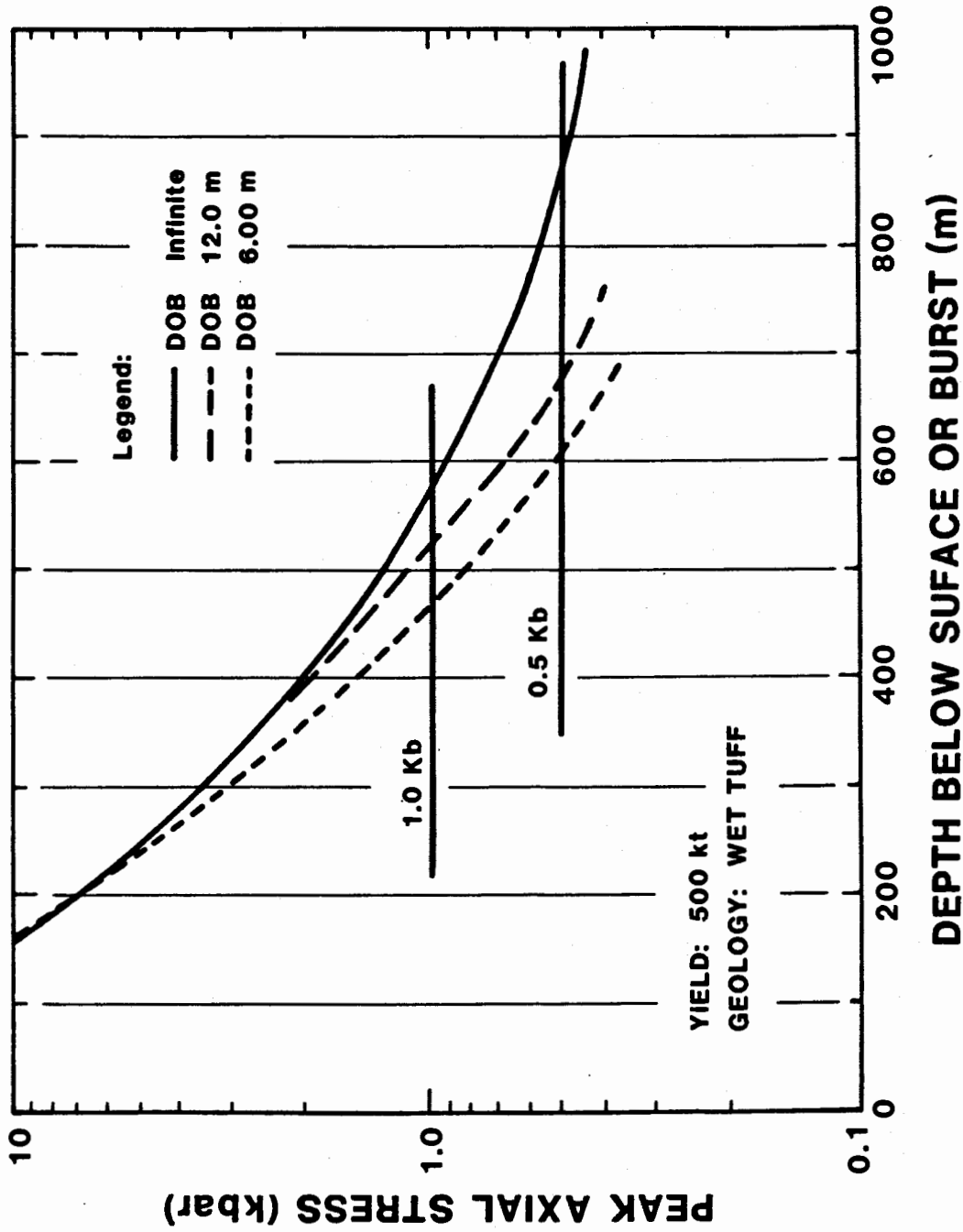


Figure 15: Peak stress on axis versus depth for EPW bursts and fully-contained explosion.

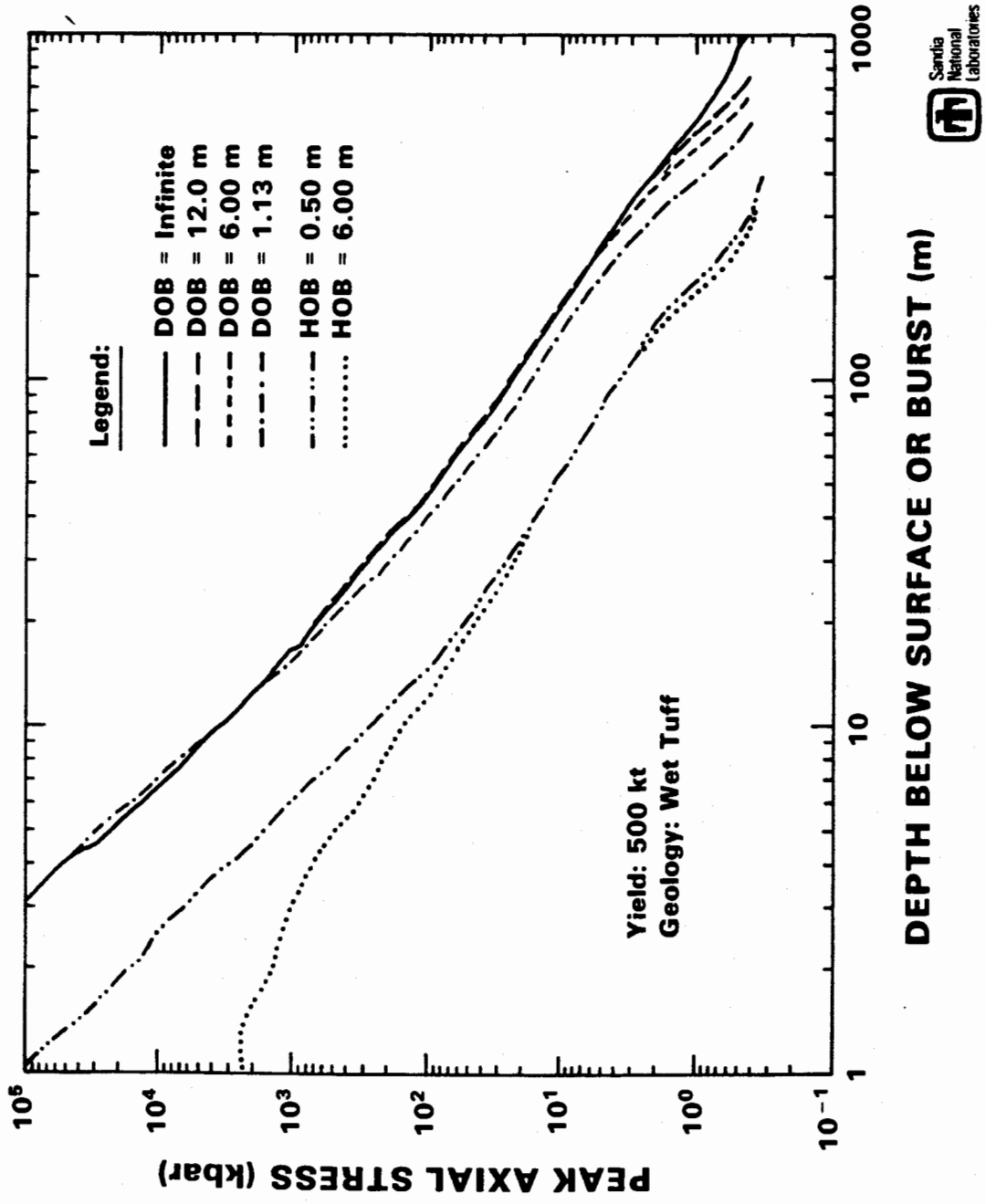


Figure 16: Peak stress attenuation on axis for EPW and near-surface bursts.



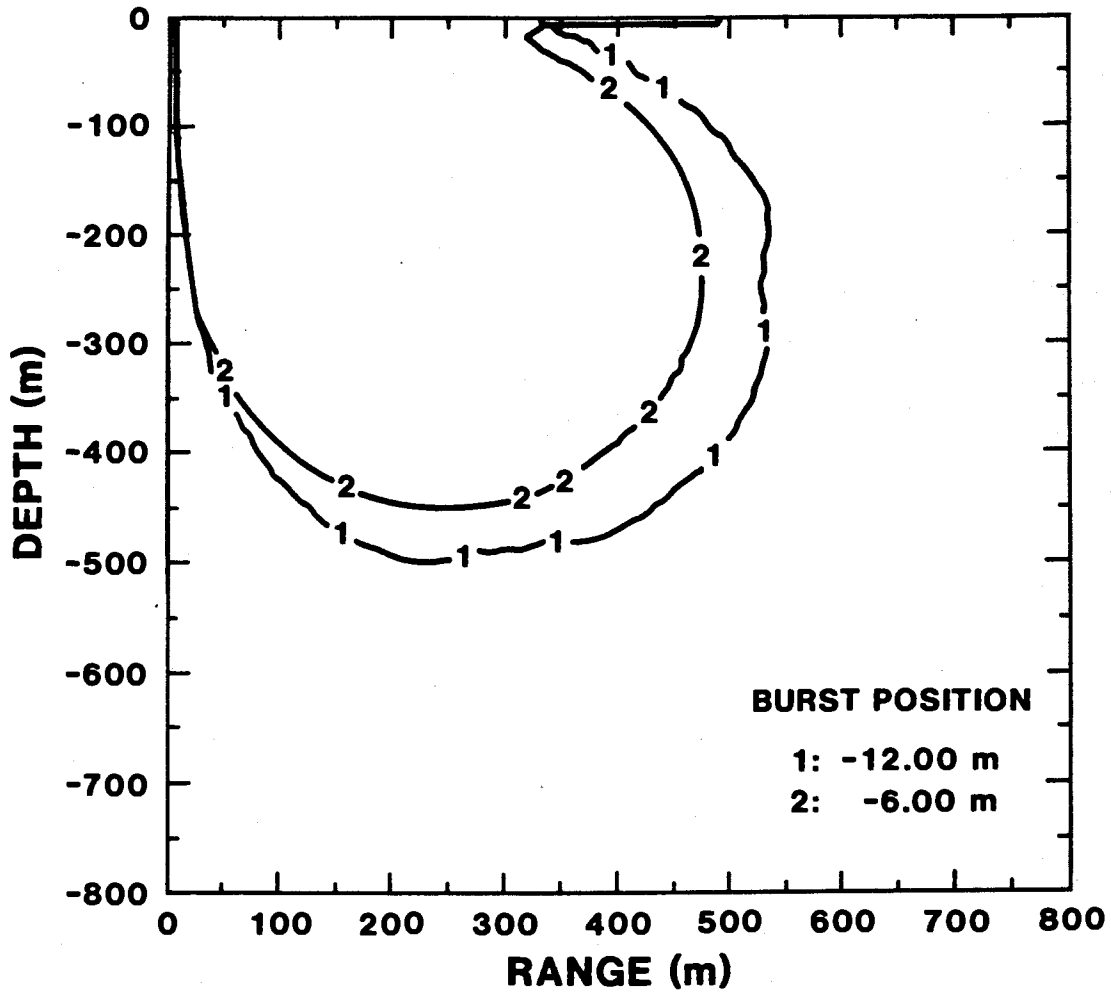


Figure 18: Comparison of 6 m/s peak horizontal velocity contours for EPW bursts.





## 6. Acknowledgements

The author wishes to acknowledge the calculational support of D. M. Webb (retired - formerly 1533) on this project and the useful comments of T. K. Bergstresser (1531) and R. A. Paulsen (9013) as reviewers of the report.



### APPENDIX

#### A. ANEOS Input for Saturated Tuff

```

-----1-----2-----3-----4-----5-----6-----7
-2          TUFF
 1.00      4.00      2.00      0.00      0.00      -2.80E+05      1.00
 1.01      2.00      1.00E+11      0.11
 1.20
 9.0  1.0

```

```

-----1-----2-----3-----4-----5-----6-----7

```

#### B. CSQII updates to provide pressure-dependent strength model for tuff

```

*ID PAULS
*I EP.716
  YVSPT1=1.49E11*(RHOI(L)-2.0)
  YVSPT2=0.30-0.30*EXP(-3.1E-09*YVSPT1)
  YVSPT2=1.0E9*YVSPT2
  IF(L.EQ.2)YOFMAT=AMIN1(YOFMAT,YVSPT2)
  YOFMAT=AMAX1(YOFMAT,0.0)

```

#### C. CSQGEN/CSQII updates to save ground shock quantities in mesh

##### C.1 CSQGEN updates

```

*ID MORST
*I GIIR.4
C IMPULSE, PEAK STRESS, AND PEAK VELOCITY UPDATES FOR CSQGEN
  NVAR=NVAR+1
  LK21=NVAR
  NVAR=NVAR+1
  LK22=NVAR

  NVAR=NVAR+1

```

LK23=NVAR  
NVAR=NVAR+1  
LK24=NVAR  
NVAR=NVAR+1  
LK25=NVAR

\*I CSQGEN.315

C LABELS FOR LINE PRINTER LISTING. NEED TO SET NEXTV1,NEXTV2,  
C OR NEXTV3 TO 21-25(YOUR CHOICE) ON CARD 4 OF CSQGEN INPUT.  
IF(L2.EQ.21) KLAB(I)=6HIMPULS  
IF(L2.EQ.22) KLAB(I)=6HMAXSY

IF(L2.EQ.23) KLAB(I)=6HMAXSXX  
IF(L2.EQ.24) KLAB(I)=6HMAXVY  
IF(L2.EQ.25) KLAB(I)=6HMAXVX

\*I CSQGEN.924

STORE(JVAR+LK21)=(AMR\*STORE(JVAR+LK21)+ANS\*FITS(5,2))/AMT  
STORE(JVAR+LK22)=(AMR\*STORE(JVAR+LK22)+ANS\*FITS(5,3))/AMT  
STORE(JVAR+LK23)=(AMR\*STORE(JVAR+LK23)+ANS\*FITS(5,4))/AMT  
STORE(JVAR+LK24)=(AMR\*STORE(JVAR+LK24)+ANS\*FITS(5,5))/AMT  
STORE(JVAR+LK25)=(AMR\*STORE(JVAR+LK25)+ANS\*FITS(5,6))/AMT

\*I CSQGEN.2654

C UPDATES FOR SUBROUTINE REZONE

IF(IK.NE.94) GO TO 201  
DUM1=DUMMY(1)  
DUM2=DUMMY(2)  
DUM3=DUMMY(3)  
DUM4=DUMMY(4)  
DUM5=DUMMY(5)  
DUMMY(1)=STORE(JVAR+LK21)  
DUMMY(2)=STORE(JVAR+LK22)  
DUMMY(3)=STORE(JVAR+LK23)  
DUMMY(4)=STORE(JVAR+LK24)

DUMMY(5)=STORE(JVAR+LK25)  
201 IF(IK.NE.95) GO TO 202  
DUMMY(1)=DUM1  
DUMMY(2)=DUM2  
DUMMY(3)=DUM3  
  
DUMMY(4)=DUM4  
DUMMY(5)=DUM5

202 CONTINUE

C.1 CSQII updates

\*ID XTRAV  
\*I CSQ.1510  
C UPDATES FOR CSQ

STORE(JVAR+LK21)=STORE(JVAR+LK21) + PZ\*DT  
SIGYYM=STORE(JVAR+LK22)  
SIGYY=PZ-STORE(JVAR+LK16)  
STORE(JVAR+LK22)=AMAX1(SIGYYM,SIGYY)  
SIGXXM=STORE(JVAR+LK23)  
SIGXX=PZ-STORE(JVAR+LK14)  
STORE(JVAR+LK23)=AMAX1(SIGXXM,SIGXX)  
VYMAX=STORE(JVAR+LK24)  
VYABS=ABS(VB)  
STORE(JVAR+LK24)=AMAX1(VYMAX,VYABS)  
VXMAX=STORE(JVAR+LK25)

VXABS=ABS(VL)  
STORE(JVAR+LK25)=AMAX1(VXMAX,VXABS)

I EP.716

YVSPT1=1.49E11\*(RHOI(L)-2.0)  
YVSPT2=0.30-0.30\*EXP(-3.1E-09\*YVSPT1)  
YVSPT2=1.0E9\*YVSPT2  
IF(L.EQ.2)YOFMAT=AMIN1(YOFMAT,YVSPT2)  
YOFMAT=AMAX1(YOFMAT,0.0)

**EXTERNAL DISTRIBUTION:**

Los Alamos National Laboratory (4)  
ATTN: T. Dey, ESS-5, MS F665  
R. Deupree, ESS-5, MS F665  
R. Weaver, X-2, MS B220  
T. Dowler, S-6, MS F601  
P. O. Box 1663  
Los Alamos, NM 87545

Lawrence Livermore National  
Laboratory (2)  
ATTN: R. Swift, MS L-200  
K. Rosenkilde, MS L-81  
P. O. Box 808  
Livermore, CA 94550

R & D Associates  
ATTN: J. Lewis  
P. O. Box 9295  
Marina del Rey, CA 90295

California Research & Technology (2)  
ATTN: A. Frederickson  
K. Kreyenhagen  
20943 Devonshire St.  
Chatsworth, CA 91311

Pacifica Technology  
Div. of Science Applications  
ATTN: R. Allen  
P. O. Box 148  
Del Mar, CA 92014

S-Cubed  
Division of Maxwell Labs  
ATTN: K. D. Pyatt  
P. O. Box 1620  
La Jolla, CA 92038-1620

Defense Nuclear Agency (2)  
ATTN: SSAB, C. McFarland  
SSAB, M. Pelkey  
Washington, DC 20305

**Sandia Internal:**

- 1510 J. W. Nunziato
- 1520 L. W. Davison
- 1530 D. B. Hayes
- 1531 S. L. Thompson
- 1531 T. K. Bergstresser
- 1533 P. Yarrington (10)
- 1533 W. T. Brown
- 1533 W. R. Davey
- 1533 A. V. Farnsworth
- 1550 C. W. Peterson
- 2300 J. L. Wirth
- 3141 S. A. Landenberger (5)
- 3151 W. I. Klein (3)
- 5110 C. C. Burks
- 5111 D. L. McCoy
- 5112 L. J. Merrill
- 5120 W. R. Reynolds
- 5160 G. R. Otey
- 5161 K. D. Nokes
- 5161 J. A. Anderson
- 5161 A. B. Cox
- 5161 J. E. Gronager
- 5165 S. D. Meyer
- 5165 W. J. Patterson
- 5166 R. C. Hartwig
- 7112 A. J. Chabai
- 8150 J. B. Wright
- 8152 J. C. Swearngen
- 8524 J. A. Wackerly
- 9010 W. C. Hines
- 9013 W. H. Ling
- 9013 R. A. Paulsen
- 9120 M. M. Newsom
- 9122 R. H. Braasch

